ZC3H11A mutations cause high myopia by triggering PI3K-AKT and NF-κB mediated inflammatory reactions in humans and mice

Chong Chen[1,2,3#], Qian Liu[1,2,3#], Yu Rong[1,2,3], Cheng Tang[1,2,3], Xinyi Zhao[1,2,3], Dandan Li[1,2,3], Fan Lu[1,2,3]*, Jia Qu[1,2,3*], Xinting Liu[1,2,3]*

[1]National Engineering Research Center of Ophthalmology and Optometry, Eye Hospital, Wenzhou Medical University, Wenzhou, 325027, China;

[2]National Clinical Research Center for Ocular Diseases, Eye Hospital, Wenzhou Medical University, Wenzhou, 325027, China;

[3]State Key Laboratory of Ophthalmology, Optometry and Visual Science, Eye Hospital, Wenzhou Medical University, Wenzhou, 325027, China.

*For correspondence: liuxt@eye.ac.cn; qujia@eye.ac.cn; lufan62@eye.ac.cn

[#] These authors contributed equally to this work.

Abstract

High myopia (HM) is a severe form of refractive error that results in irreversible visual impairment and even blindness. However, the genetic and pathological mechanisms underlying this condition are not yet fully understood. From a adolescents myopia survey cohort of 1015 HM patients, pathogenic missense mutations were identified in the ZC3H11A gene in four patients by whole exome sequencing. This gene is a zinc finger and stress-induced protein that plays a significant role in regulating nuclear mRNA export. To better understand the function and molecular pathogenesis of myopia in relation to gene mutations, a Zc3h11a knock-out (KO) mouse model was created. The heterozygous KO (Het-KO) mice exhibited significant shifts in vision towards myopia. Electroretinography revealed that the b-wave amplitude was significantly lower in these mice under dark adaptation. Using immunofluorescence antibodies against specific retinal cell types, the density of bipolar cell-labelled proteins was found to be decreased. Transmission electron microscopy findings suggesting ultrastructural abnormalities of the retina and

sclera. Retinal transcriptome sequencing showed that 769 genes were differentially expressed, and Zc3h11a was found to have a negative impact on the PI3K-AKT and NF-κB signalling pathways by quantitative PCR and western blotting. In addition, myopia-related factors, including TGF-β1, MMP-2 and IL-6 were found to be upregulated in the retina or sclera. In summary, this study characterized a new pathogenic gene associated with HM. The findings indicated that the ZC3H11A protein may serve as an innate immune and inflammatory response trigger, contributing to the early onset of myopia. These findings offer potential therapeutic intervention targets for controlling the development of HM.

Introduction

Myopia is a highly prevalent eye affliction that commonly develops during childhood and early adolescence. The prevalence of myopia among the adult population ranges from 10-30%, while parts of East and Southeast Asia have reported rates as high as 80-90% among young people (Baird et al., 2020; Holden et al., 2016). HM is a severe refractive error characterised by a diopter ≤ -6.00 D or an ocular axis greater than 26 mm. It is estimated that by 2050, the number of people with HM worldwide will reach 938 million, accounting for 9.8% of the total population. HM can trigger a range of adverse ocular changes, such as cataracts, glaucoma, retinal detachment, macular degeneration and possibly total blindness (Koga et al., 2014; Saw et al., 2005). While conventional methods for the prevention and control of myopia can provide some correction, they are not entirely effective in managing its progression, particularly during childhood and adolescence.

With the development of next-generation sequencing, whole exome sequencing (WES) and whole genome sequencing (WGS) have extended the findings of linkage studies to identify potential causes of syndromic HM (sHM) and non-syndromic HM (nsHM). To date, approximately 20 genes with causal associations have been identified in sHM, including ZNF644, SCO2, CCDC111, LRPAP1, SLC39A5, LEPREL1, P4HA2, OPN1LW, ARR3, BSG, NDUFAF7, CPSF1, TNFRSF21, DZIP1, XYLT1, CTSH, GRM6, LOXL3 and GLRA2 (Haarman et al., 2022; Tian et al., 2023;

Yang et al., 2023; Ye et al., 2023). These discoveries have provided insight into the molecular mechanisms underlying HM. However, known candidate genes can only explain about 20% of the causes of this disease (Cai et al., 2019; Tedja et al., 2019). At the same time, the neuromodulators and signal molecules of HM are extremely complex, including sclera extracellular matrix (ECM) remodelling and endoplasmic reticulum (ER) stress (Ikeda et al., 2022), inflammatory responses, the release of dopamine and gamma-aminobutyric acid (GABA), or abnormalities in myopia-related signalling pathways, such as retinoic acid signalling, TGF-β signalling and HIF-1α signalling.

Screening mutations from a adolescents myopia survey cohort by WES, we identified zinc finger CCCH domain-containing protein 11A (ZC3H11A) as a HM candidate gene. This particular gene is a member of the zinc finger protein gene family. Several of its members have been linked to myopia or HM, including ZNF644, ZC3H11B, ZFP161 and ZENK. Like ZC3H11B, a gene that is conserved with respect to ZC3H11A in humans, the five genome-wide variants loci have previously been found to be strongly associated with greater axial length (AL) or HM (Schippert et al., 2007; Shi et al., 2011; Szczerkowska et al., 2019; Tang et al., 2020; Wang et al., 2004). Recent proteomic studies have indicated that ZC3H11A may be a constituent of the transcriptional export (TREX) complex. Additionally, it has been suggested that this protein is involved in stress-induced responses (Younis et al., 2018). Dysfunction of ZC3H11A results in enhanced NF-κB signalling through defective IκBα protein expression, which is accompanied by upregulation of numerous innate immune- and inflammation-related mRNAs, including IL-8, IL-6 and TNF in vitro (Jimi et al., 2019). Moreover, patients with myopia have a higher proportion of inflammation-associated cells, including neutrophils, while those with moderate myopia show strained immune system function (Lin et al., 2016; Qi et al., 2022). Conversely, some traditional Chinese medicines can control myopia progression by suppressing AKT and NF-κB mediated inflammatory reactions (Chen et al., 2022). However, the precise pathological mechanism of ZC3H11A in myopia development remains unclear, necessitating further research.

The current study identified four HM-related variants in the ZC3H11A gene among a cohort of 1015 adolescents. Additionally, KO mice were constructed using the CRISPR/Cas9 system and their myopic phenotypes, visual function, bipolar cell apoptosis, and retinal and scleral microstructure were assessed. Moreover, RNA sequencing and expression experiment was performed to identify perturbed molecules and pathways and to examine the interactions between these factors in relation to HM. The above results will provide new ideas for the prevention and control of high myopia, especially early-onset, uncorrectable and familial myopia.

Results

ZC3H11A mutations are associated with HM in a Chinese cohort

The subjects were selected from the Myopia Associated Genetics and Intervention Consortium (MAGIC), our previously published research involving large-scale myopia cohorts and genomic sequencing data. Four missense mutations in the ZC3H11A gene (c.412G>A, p.V138I; c.128G>A, p.G43E; c.461C>T, p.P154L; and c.2239T>A, p.S747T) were identified in the 1015 HM patients aged from 15 to 18 years. The uncorrected visual acuity (UCVA) and ocular axial length of these patients are presented in Table 1. A tessellated fundus was observed in patient 1 and patient 3. All of the identified mutations exhibited very low frequencies in the Exome Aggregation Consortium (ExAC) or Genome Aggregation Database (gnomAD), with CADD > 22.7. Among them, c.412G>A, c.128G>A and c.461C>T were located in or around a domain named zf-CCCH_3 (Figure 1A and B). Furthermore, all of the mutation sites were located in highly conserved amino acids across different species (Figure 1C). Four mutations resulted in a higher degree of conformational flexibility and altered the negative charge at the corresponding sites (Figure 1D and E).

Zc3h11a Het-KO mice exhibited myopic phenotypes

Het-KO mice were constructed at four weeks of age against a C57BL/6J background using CRISPR/Cas9 technology (Figure supplement 1). Retinal fundus images and ocular histomorphology of Zc3h11a Het-KO mice at eight weeks postnatal were

assessed against those of their wild-type (WT) counterparts. No significant structural differences were observed (Figure supplement 2). These findings suggest that the deletion of Zc3h11a does not alter the retinal structure or ocular histomorphology. Therefore, Zc3h11a Het-KO mice are a relevant model for the investigation of the role of Zc3h11a in refractive development.

Refraction and axial length in Zc3h11a Het-KO mice were found to be significantly greater than in WT littermates (independent samples t-test, $p<0.05$; Figure 2A and B). The difference between the two genotypes was statistically significant at weeks 4 and 6. Correspondingly, the vitreous chamber depth of Zc3h11a Het-KO mice was deeper than that of WT littermates (independent samples t-test, $p<0.05$; Figure 2C). There were no significant differences in the anterior chamber depth, lens diameter and body weight between the two groups (Figure 2D-F). These results suggest that the Het-KO of the Zc3h11a gene may lead to an increase in myopia in mice.

Reduced b-wave amplitude and bipolar cell-labelled protein density in Zc3h11a Het-KO mice

To confirm if Zc3h11a is responsible for refractive development regulation, visual function was assessed by electroretinography (ERG). Upon dark adaptation, b-wave amplitudes in seven-week-old Het-KO mice were significantly lower at dark 3.0 and dark 10.0 compared to WT mice (Figure 3A and C). On the contrary, there were no differences in a-wave amplitudes between the Het-KO and WT groups (Figure 3B). Based on the ERG results, variations between Het-KO and WT littermates can be observed. The ERG b-wave, predominantly generated by bipolar cells, was significantly modified in both the 3.0 and 10.0 dark adaptation conditions. Immunofluorescence analyses were performed on frozen retinal sections to investigate this phenomenon further. Specifically, Zc3h11a, PKCα, Opsin-1 and Rhodopsin markers were utilised to detect the Zc3h11a protein, rod-bipolar cells, cone cells and rod cells, respectively (Figure 3D-F). Additionally, the differences in the Zc3h11a and PKCα protein contents of the retina were quantified through western blot analysis. Notably, the protein densities of Zc3h11a and PKCα were decreased in

150 the Het-KO group (Figure 3G and H). However, there were no significant differences
151 in the densities of cone and rod cells between the two groups (Figure 3I and J).
152
153 **Retinal ultrastructure alterations in het-KO mice model**
154 Transmission electron microscopy (TEM) was used to analyse retinal ultrastructure of
155 in 10-week-old mice. In the inner nuclear layer (INL) of the retina, in contrast to WT
156 mice, Het-KO mouse cells had enlarged perinuclear gaps (black arrow), perinuclear
157 cytoplasmic oedema (blue arrow), and thinned and lightened cytoplasm (Figure 4A
158 and B). However, in the outer nuclear layer (ONL), no significant difference in cell
159 morphology was observed between the two groups of mice (Figure 4C and D).
160 Furthermore, when compared to the WT group, the Het-KO mice exhibited relatively
161 damaged photoreceptor cell membrane discs (MB), in which the outer layer was
162 detached and sparsely distributed locally (Figure 4E and F). There were also a small
163 number of broken membrane discs, as well as some disorganized and loosely arranged
164 ones (red arrow), with a slight increase in size (Figure 4G and H).
165
166 **RNA-Seq analysis of molecular and pathways changes in Zc3h11a Het-KO mice**
167 **retinas**
168 In the retina transcriptome analysis, 769 genes were differentially expressed (Fold
169 change (FC) of at least two and a P value < 0.05) in the Zc3h11a Het-KO group, of
170 which, 303 were upregulated and 466 were downregulated (Figure 5A and B). GO
171 enrichment analysis revealed that these were primarily involved in biological
172 processes (such as zinc ion transmembrane transport, RNA biosynthetic and metabolic
173 process, and negative regulation of NIK/NF-κb signalling) and molecular functions
174 (such as calcium ion binding and zinc ion transmembrane transporter activity) (Figure
175 5C and D). KEGG pathway enrichment analysis indicated that the differentially
176 expression genes (DEGs) in the Zc3h11a Het-KO group were primarily involved in
177 the PI3K-AKT signalling pathway, MAPK signalling pathway, human virus infection
178 and neuropsychiatric disease (Figure 5E).
179

Zc3h11a negatively regulates the PI3K-AKT and NF-κB pathways

PI3K-AKT is one of the most important pathways for cell survival, division, autophagy and differentiation (Alzahrani, 2019). Meanwhile, it has been found that ZC3H11A can regulate the NF-κB pathway at the level of IκB mRNA export in ZC3-KO cells (Darweesh et al., 2022). IκBα is a critical protein that governs NF-κB function predominantly within the cytoplasmic compartment. It plays a pivotal role in inhibiting the activation of NF-Kb (Dyson and Komives, 2012; Manavalan et al., 2010). In addition, AKT promotes IκBα phosphorylation to undergo degradation, which enhances the nuclear translocation of NF-kB (Alzahrani, 2019; Torrealba et al., 2020). Accordingly, we investigated whether ZC3H11A has any regulatory influence on the transcriptional activation of PI3K-AKT and NF-κB *in vivo*. To this end, we evaluated the mRNA and protein expression levels of ZC3H11A, PI3K, AKT, p-AKT, IκBα and NF-κB in the retina. The expression levels of ZC3H11A, PI3K, AKT, p-AKT and NF-κB were significantly upregulated, while IκBα was downregulated in Het-KO mice (Figure 6A-L). These findings strongly suggest that ZC3H11A exerts a negative impact on the PI3K-AKT and NF-κB pathways.

TGF-β1, MMP-2 and IL-6 were increased in Zc3h11a Het-KO mice

In animal models of myopia, it has been established that intraocular concentrations of TGF-β1 are elevated (Chen et al., 2013; Liu et al., 2022), especially in the retina and sclera. The abnormal expression of matrix metalloproteinase-2 (MMP-2) and interleukin-6 (IL-6) can induce myopia, and these are regulated by NF-κB (Libermann and Baltimore, 1990; Wu and Schmid-Schönbein, 2011). To investigate the hypothesis that the TGF-β1 and NF-κB signalling pathways exhibit hyperactivity in the retina in the presence of reduced Zc3h11a, we assessed the expression of TGF-β1, MMP-2 and IL-6 at the mRNA levels in the retina and sclera of WT and Het-KO mice, while analysing scleral TEM. Additionally, we confirmed changes in the expression levels of TGF-β1 and MMP-2 in the retina at the protein level. qPCR analysis showed increased expression of TGF-β1, MMP-2, and IL-6 in the sclera and retina of Het-KO mice compared with WT mice (Figure 7A and B). Scleral TEM results suggested that

scleral collagen fibres in Het-KO mice were disorganized over a large area with irregular transverse and longitudinal arrangement (Figure 7C). The western blot results showed increased expression levels of TGF-β1 and MMP-2 in the retinas of Zc3h11a Het-KO mice (Figure 7D).

Discussion

This study identified and validated a new candidate gene in a large high myopia cohort, ZC3H11A. Moreover, the study provided evidence of the presence of moderate or HM phenotypes and damaged bipolar cells *in vivo* by constructing Het-KO mice for the first time. TEM analysis showed ultrastructural changes in parts of both the retina and sclera of Het-KO mice. To understand how ZC3H11A regulates the development of HM, retinal transcriptome sequencing was performed. The results revealed that Zc3h11a upregulates the PI3K-AKT and NF-κB signalling pathways. In addition, the expression levels of myopia-related factors, such as TGF-β1, MMP-2 and IL-6, were upregulated in the retina and sclera of the Het-KO mice. Therefore, it can be speculated that the ZC3H11A protein may act as an innate immune and inflammatory response trigger, contributing to the early onset of HM.

ZC3H11A is involved in the export and post-transcriptional regulation of selected mRNA transcripts required to maintain metabolic processes in embryonic cells; these are essential for the viability of early mouse embryos (Younis et al., 2023). In studies of chickens, mice and humans, the zinc finger protein ZENK was found to play a role in the development of refractive myopic excursion and lengthening of the ocular axis. Moreover, early growth response gene type 1 Egr-1 (the human homolog of ZENK) activates the TGF-β1 gene by binding to its promoter, which is thought to be associated with myopia (Baron et al., 2006; Xiao et al., 2022). Another zinc protein finger protein 644 isoform, ZNF644, has recently been identified by WES as causing HM in Han Chinese families (Shi et al., 2011). ZC3H11A is also a zinc finger protein, and the findings of the current study revealed that Zc3h11a Het-KO mice showed a myopic shift, which is consistent with previous studies reporting reduced protein expression of Zc3h11a in an unilateral induced myopic mouse model (Fan et al.,

240 2012).

241 In vertebrate models, refractive development and ocular axial growth are visually
242 controlled (Wallman and Winawer, 2004). The regulation of axial length or refractive
243 error occurs through complex light-dependent retina-to-sclera signalling (Tkatchenko
244 and Tkatchenko, 2019). Optical scatter information is processed by the retina and then
245 converted into molecular signals that regulate peripheral retinal growth and scleral
246 connective tissue renewal, ultimately affecting the growth rate of the posterior
247 segment of the eye (Harper and Summers, 2015; Tkatchenko et al., 2006; Tkatchenko
248 et al., 2018). All cell types of the retina contain myopia-related genes and retinal
249 circuitry driving refractive error. In this study, Het-KO mice were found to have
250 reduced b-wave amplitudes, diminished relative fluorescence intensity of bipolar cells
251 and ultrastructural changes in inner nuclear layer (INL) of the retina. Therefore, it is
252 presumed that retinal circuitry changes result in impairment of visual signal
253 processing and transduction causing HM.

254 Aberrant activation of the PI3K-AKT and NF-κB signalling pathways has been
255 identified in highly myopic retinas. Following the sequencing evidence indicating
256 elevations in PI3K-AKT and NF-κB signalling (Lin et al., 2016), we sought to explore
257 the potential interplay between these pathways in mice. The results revealed that a
258 decrease in Zc3h11a inhibited the translocation of IκBα from the nucleus to the
259 cytoplasm. IκBα is a downstream factor of PI3K-AKT and binds to NF-κB (p65) in
260 the cytoplasm, inhibiting its nuclear translocation. The qPCR and western Blot results
261 verified that Zc3h11a negatively regulates both the PI3K-AKT and NF-κB signalling
262 pathways. Thus, Zc3h11a may exert an influence on these pathways by modulating
263 the cytoplasmic levels of IκBα, contributing to the development of myopia.

264 NF-κB was first discovered 25 years ago and described as a key regulator of induced
265 gene expression in the immune system, playing a central role in the coordinated
266 control of intrinsic immune and inflammatory responses (Hayden and Ghosh, 2011;
267 Morgan and Liu, 2011). The downstream factors of this pathway include IL-6, IL-8,
268 TNF-α, MMP-2, TGF-β1, etc (Jimi et al., 2019; Yoshida and Whitsett, 2006). Studies
269 have demonstrated that the MMP-2 and IL-6 expression levels are increased in

myopic eyes and that inhibiting MMP-2 or IL-6 expression will provide some degree of control over myopia progression (Lin et al., 2016; Zhao et al., 2018). Identification of the PI3K-AKT-NF-κB signalling pathway and downstream myopia effect in our study may open up new opportunities for the prevention and treatment of HM and fundus lesions in the future.

There are a number of limitations of this study that should be acknowledged. First, Zc3h11a homozygous KO (Homo-KO) mice were not obtained in our study because homozygous deletion of exons may confer embryonic lethality (Younis et al., 2023). Second, while the current study observed a reduced b-wave amplitude and bipolar cell fluorescence staining intensity in Het-KO mice, an in-depth exploration of the underlying mechanism was beyond the scope of the research. Finally, there was a limited observation time in this study and the effect of ZC3H11A on the late refractive system was not assessed.

Overall, this study has provided four key findings. First, it was confirmed that the ZC3H11A is a new candidate gene is associated with HM in a cohort of Chinese Han individuals. Secondly, changes in Zc3h11a expression were found to affect retinal function, particularly in bipolar cells. Third, changes in Zc3h11a expression were found to cause alterations in numerous signalling pathways, the most notable being the PI3K-AKT and NF-κB pathways. Fourth, changes in Zc3h11a expression were found to cause changes in the myopia-related genes TGF-β1, MMP-2 and IL-6. The above results suggest that Zc3h11a promotes the translocation of IκBα from the nucleus to the cytoplasm, thereby exerting negative feedback regulation of the PI3K-AKT signalling pathway and inhibiting the NF-κB signalling pathway. At the same time, the increase in TGF-β1 in myopic eyes stimulates the PI3K-AKT signalling pathway, which leads to activation of the PI3K-AKT signalling pathway, resulting in downstream degradation of IκBα after phosphorylation. This, in turn, increases the nuclear translocation of NF-κB. To sum up, Zc3h11a promotes the myopia-associated factor TGF-β1 by acting directly or indirectly on both the PI3K-AKT and NF-κB signalling pathway-mediated inflammatory reactions and the expression of MMP-2 and IL-6, which together, promote the development of early myopia (Figure 8).

Therefore, this model can be used as one of the new strategies for intervention and treatment of high myopia. However, because the causes of myopia or HM are complex and involve different tissues and molecular pathways in the eye, it is likely that future research will identify more genes and molecular mechanisms that could provide guidance for clinical intervention and treatment.

Materials and methods

Ethics approval and consent to participate

The studies that involved human participants were approved by the Eye Hospital, Wenzhou Medical University (Wenzhou, China), and were carried out in strict adherence to the guidelines of the Helsinki Declaration. All participants provided informed consent. Furthermore, all animal experiments were approved by the Animal Care and Ethics Committee at Wenzhou Medical University and were performed according to the guidelines set forth in the Association for Research in Vision and Ophthalmology Statement for the Use of Animals in Ophthalmic and Visual Research. (https://www.arvo.org/About/policies/statement-for-the-use-of-animals-in-ophthalmic-and-vision-research/).

Recruitment of subjects

A total of 1015 sporadic HM patients were recruited from the Eye Hospital of Wenzhou Medical University for MAGIC project. HM was defined as SE ≤ -6.00 D in either eye (Flitcroft et al., 2019). Detailed ophthalmic examinations, including visual acuity, axial length, slit-lamp, fundus photography and optical coherence tomography were performed.

WES and the detection of variants

DNA was extracted from all probands using a FlexiGene DNA Kit (Qiagen, Venlo, The Netherlands), according to the manufacturer's protocol. DNA from all probands underwent WES using a Twist Human Core Exome Kit and an Illumina NovaSeq 6000 sequencing system (150PE) (Berry Genomics Institute, Beijing, China). The

330 mean depth and coverage of the target region were approximately 78.26× and 99.7%,
331 respectively. Sequence reads were aligned to the reference human genome (UCSC
332 hg19) using the Burrows-Wheeler aligner (BWA). The variants were called and
333 annotated with Verita Trekker and Enliven software (Transcript ID,
334 ENST00000332127.4, Berrry Genomics Institute), respectively.
335
336 **Het-KO mice model construction, husbandry and ocular biometric**
337 **measurements**
338 Het-KO mice were constructed at four weeks of age against a C57BL/6J background
339 using CRISPR/Cas9 technology at GemPharmatech Co.,Ltd (Nanjing, China). Exon5-
340 exon6 of the Zc3h11a transcript was recommended as the KO region; this region
341 contains a 244bp coding sequence. Littermates of Het-KO and WT mice were used
342 for all experiments. All animals were housed in the animal husbandry room of
343 Wenzhou Medical University. Mice were housed in standard transparent mouse cages
344 at 22±2°C with a 12-hour light/12-hour dark cycle (light from 8 am to 8 pm,
345 brightness approximately 200-300 lux) and free access to food and water. To exclude
346 the effect of ocular developmental malformations, mice with small eyes and ocular
347 lesions were excluded from the observation cohort. Body weight, refraction and
348 ocular biometrics of Het-KO (n=14) and WT (n=10) mice were assessed at 4, 5, 6, 8
349 and 10 weeks of age.
350
351 **Electroretinography**
352 To evaluate the effect of Zc3h11a on the electrophysiological properties of various
353 neuronal populations in the retina, ERG was performed on the right eye of Het-KO
354 and WT littermates at seven weeks of age, at the same time of day (n=12). Both
355 scotopic and photopic ERG responses were evaluated. The mice were dark-adapted
356 overnight, and all procedures were performed under dim red light (<1 lux). The
357 animals were anaesthetized with intraperitoneal injection of pentobarbital sodium (40
358 mg/kg) and the pupils were dilated with 0.5% tropicamide. A heating table (37°C) was
359 used to maintain body temperature. ERG was recorded using a Roland

360 Electrophysiological System (RETI-Port21, Roland Consult, Germany) with ring-
361 shaped corneal electrodes. Three light intensities (0.01, 3.0 and 10.0 cds/m^2) were
362 applied to each animal. The following parameters were measured: a-wave amplitude
363 and b-wave amplitude. Photopic ERG was measured at a light intensity of 3.0 cds/m^2
364 after 10 min light adaption at 25 cds/m^2. The responses of the Het-KO eyes (right)
365 were compared with those of the WT eyes (right).
366
367 **Immunofluorescence**
368 Whole mouse eyes (10 weeks, littermates Het-KO and WT) were fixed with 4% para-
369 formaldehyde (BL539A, Biosharp, China) for 1 h and 30% sucrose for dehydration
370 overnight. Then, they were fabric-embedded in a frozen fabric matrix compound at -
371 20℃. Prepared tissue blocks were segmented with a cryostat at a thickness of 12
372 microns and collected on clean adhesive slides. The slices containing the sections
373 were air-dried at room temperature (RT) for 15 min. After washing 3× with 1× PBS
374 for 5 min, 5% BSA (SW3015, Solarbio, China) and 0.03% triton-X100 (P0096,
375 Beyotime, China) diluted with 1× PBS were added as permeable membrane-blocking
376 buffers. The slides were incubated for 1 h at RT in a humid chamber. Then, they were
377 incubated overnight at 4℃ with the specific primary antibody Zc3h11a (1:50, 26081,
378 Proteintech, USA). PKC α (1:200, ab32518, Abcam, UK), Opsin-1 (1:200, NB110-
379 74730, Novus Biologicals, USA) and Rhodopsin (1:200, NBP2-25160, Novus
380 Biologicals, USA) were added and the slices were incubated further at 4℃ in a humid
381 chamber overnight. After washing 4× with 1× PBS for 6 min, goat anti-rabbit Alexa
382 Fluor 488 (1:500, ab150077, Abcam, UK) was added and the slides were incubated
383 for 90 min at RT. After washing, the slides were mounted with an antifade medium
384 containing DAPI (P0131, Beyotime, China) to visualize the cell nucleus. Sections
385 incubated with 5% BSA and without primary antibodies were used as negative
386 controls. A fluorescence microscope (LSM 880, ZEISS, Germany) was used to
387 examine the slides and capture images. The experiments were repeated in duplicate
388 with three different samples.
389

390 **Transmission electron microscopy**

391 At 10 weeks of age, two mice of each genotype were euthanized, and their eyes were
392 removed. The eyes were fixed in a solution containing 2.5% glutaraldehyde and 0.01
393 M phosphate buffer (PB) (pH 7.0-7.5) for 15 min while the optic cups were dissected.
394 The optic cups were then fixed with 1% osmium acid at room temperature away from
395 light for 2h, after which they were rinsed three times with 0.1 MPB for 15min each
396 time. Tissues were sequentially dehydrated in 30%-50%-70%-80%-95%-100%-100%
397 ethanol upstream for 20 min each time, and 100% acetone twice for 15 min each time.
398 Finally, the tissues were embedded in epoxy resin (Polybed 812) mixed 1:1 with
399 acetone. Ultrathin sections were prepared using diamond knives and an EM UC7
400 ultramicrotome (Leica, Germany), then the sections were stained with 2% aqueous
401 dioxygen acetate and 1% phosphotungstic acid (pH 3.2). Finally, the structures were
402 examined using a transmission electron microscope (HT7700, Hitachi, Tokyo, Japan).

403

404 **RNA sequencing analysis of molecular and pathway changes in the mouse retina**

405 Mice aged four weeks were executed by cervical dislocation after CO2 asphyxiation.
406 Then, the eyes were enucleated and dissected to obtain the entire retinas. Three eye
407 retinas from the Zc3h11a Het-KO and WT groups were used for the mRNA
408 sequencing experiments and performed by Biomarker Biotechnology Co. (Beijing,
409 China). The mRNA sequences were mapped to the genome (GRCm38). WebGestalt
410 (http://www.webgestalt.org/) was used to generate GO terms and KEGG pathways.

411

412 **qRT-PCR**

413 To determine the reliability of the transcriptome results, qPCR validation was
414 performed. RNA was isolated using Trizol reagent (RC112, Vazyme, China), and the
415 purity was confirmed by the OD260/280 nm absorption ratio (1.9-2.1) (Nanodrop
416 2000, Thermo Scientific, USA). Total RNA (2 μg) was reverse transcribed to cDNA
417 using a cDNA Synthesis Kit (R323, Vazyme, China). qPCR was performed with a RT-
418 PCR detection system (Applied Biosystems, California, USA) using a SYBR Premix
419 Ex Taq Kit (Q711, Vazyme, China), according to the manufacturer's instructions.

420 qRT-PCR was performed (ABI-Q6, California, USA) in a 20 μL reaction, under the
421 following conditions: 95°C for 10 min, followed by 40 cycles of amplification at
422 95°C for 10 s and 60°C for 60 s. Melting curve analysis was used to determine
423 specific amplification. All experiments were performed in triplicate. Relative
424 quantification was performed using the ΔΔCt method. The specific gene products
425 were amplified using the following primer pairs (Table supplement 1).
426
427 **Western blot**
428 The mouse retina was separated immediately after enucleation of the eyeball and
429 lysed in RIPA (10 mM Tris-Cl, 100 mM NaCl, 1 mM EDTA, 1 mM NaF, 20 mM
430 $Na_4P_2O_7$, 2 mM Na_3VO_4, 1% Triton X-100, 10% glycerol, 0.1% sodium dodecyl
431 sulphate and 0.5% deoxycholate) lysis buffer containing protease and phosphatase
432 inhibitors (P1045, Beyotime, China). Equal amounts of protein (15 μg) were
433 separated on 10% Tris-glycine gel, transferred to PVDF (polyvinylidene fluoride)
434 membranes, and blocked with 5% skim milk. The primary antibodies used included
435 ZC3H11A (ab99930, Abcam, UK), AKT (#4691, Cell Signaling Technology, USA),
436 p-AKT (#4060, Cell Signaling Technology, USA), IκBα (ab32518, Abcam, UK), NF-
437 κB (ab32536, Abcam, UK), TGF-β1 (21898, Proteintech, USA) and MMP-2
438 (ab92536, Abcam, UK) diluted to 1:1000 in TBST-5% milk. Then, the membranes
439 were incubated with goat anti-rabbit IgG conjugated with HRP (1:2000 in TBST-5%
440 milk) (SA00001-2, Proteintech, USA) for 90 min at room temperature and developed
441 using western blotting reagents (BL523B, Bioshark, China). GAPDH (AF2823,
442 Byotime, China) was used as the internal control.
443
444 **Software and statistical analysis**
445 All experiments were repeated at least once, and sample sizes and reported results
446 reflect the cumulative data for all trials of each experiment. Each result is expressed
447 as the mean ± standard deviation (SD). Pearson's test was used to assess the normality
448 of the data. The normally distributed data were subjected to parametric analyses.
449 Unpaired Student's t-tests were used for parametric analyses between two groups.

Data that were not normally distributed or had a sample size that was too small, were subjected to nonparametric analyses. Nonparametric tests between two groups were performed using the Wilcoxon signed-rank test for matched pairs, the Mann-Whitney U-test or the Kruskal-Wallis test for multiple comparisons (GraphPad Prism 9, La Jolla, CA). A difference was considered statistically significant when the p-value was less than 0.05 and highly significant if it was less than 0.01 or less than 0.001.

Acknowledgements

The authors wish to thank all of the members of our lab. Additionally, we thank Xiangtian Zhou (Eye Hospital, Wenzhou Medical University) and Institute of PSI Genomics Co., Ltd for their technical assistance.

Additional information

Funding

This work was supported by the National Natural Science Foundation of China (82101176), Key Research and Development Program of Zhejiang Province (2021C03102), Natural Science Foundation of Zhejiang Province (LTGD23H120002), National Key Research and Development Program for Active Health and Aging Response (2020YFC2008200), and Health Technology Plan Project in Zhejiang Province (2021KY808).

Author Contributions

Conceptualisation, Xinting Liu, Jia Qu and Fan Lu; methodology, Chong Chen and Qian Liu; data analysis, Chong Chen, Qian Liu, Cheng Tang and Yu Rong; investigation and cohort construction, Xinting Liu, Jia Qu, Fan Lu, Dandan Li and Xinyi Zhao; writing original draft preparation, Chong Chen, Qian Liu and Xinting Liu; writing-review and editing, Xinting Liu, Jia Qu and Fan Lu; funding acquisition, Xinting Liu, Jia Qu and Fan Lu. All authors have read and agreed to the published version of the manuscript.

Ethics approval

The study was approved by the Institutional Review Board of Eye Hospital, Wenzhou Medical University, Zhejiang, China (Approval number: 2019-215-K-192). Informed consent was obtained from each subject. The study was approved by the Animal Care and Ethics Committee at Wenzhou Medical University (Wenzhou, China).

Data availability

All data generated or analysed during this study are included in the manuscript and supporting files.

References

Alzahrani, A.S., 2019. PI3K/Akt/mTOR inhibitors in cancer: At the bench and bedside. Semin Cancer Biol 59, 125-132.

Baird, P.N., Saw, S.M., Lanca, C., Guggenheim, J.A., Smith Iii, E.L., Zhou, X., Matsui, K.O., Wu, P.C., Sankaridurg, P., Chia, A., Rosman, M., Lamoureux, E.L., Man, R., He, M., 2020. Myopia. Nat Rev Dis Primers 6, 99.

Baron, V., Adamson, E.D., Calogero, A., Ragona, G., Mercola, D., 2006. The transcription factor Egr1 is a direct regulator of multiple tumor suppressors including TGFbeta1, PTEN, p53, and fibronectin. Cancer Gene Ther 13, 115-124.

Cai, X.-B., Zheng, Y.-H., Chen, D.-F., Zhou, F.-Y., Xia, L.-Q., Wen, X.-R., Yuan, Y.-M., Han, F., Piao, S.-Y., Zhuang, W., Lu, F., Qu, J., Yu, A.Y., Jin, Z.-B., 2019. Expanding the Phenotypic and Genotypic Landscape of Nonsyndromic High Myopia: A Cross-Sectional Study in 731 Chinese Patients. Invest Ophthalmol Vis Sci 60, 4052-4062.

Chen, B.-Y., Wang, C.-Y., Chen, W.-Y., Ma, J.-X., 2013. Altered TGF-β2 and bFGF expression in scleral desmocytes from an experimentally-induced myopia guinea pig model. Graefes Arch Clin Exp Ophthalmol 251, 1133-1144.

Chen, C.-S., Hsu, Y.-A., Lin, C.-H., Wang, Y.-C., Lin, E.-S., Chang, C.-Y., Chen, J.J.-Y., Wu, M.-Y., Lin, H.-J., Wan, L., 2022. Fallopia Japonica and Prunella vulgaris inhibit myopia progression by suppressing AKT and NFκB mediated inflammatory reactions. BMC Complement Med Ther 22, 271.

509 Darweesh, M., Younis, S., Hajikhezri, Z., Ali, A., Jin, C., Punga, T., Gupta, S., Essand,
510 M., Andersson, L., Akusjärvi, G., 2022. ZC3H11A loss of function enhances NF-κB
511 signaling through defective IκBα protein expression. Front Immunol 13, 1002823.
512 Dyson, H.J., Komives, E.A., 2012. Role of disorder in IκB-NFκB interaction. IUBMB
513 Life 64, 499-505.
514 Fan, Q., Barathi, V.A., Cheng, C.-Y., Zhou, X., Meguro, A., Nakata, I., Khor, C.-C.,
515 Goh, L.-K., Li, Y.-J., Lim, W.e., Ho, C.E.H., Hawthorne, F., Zheng, Y., Chua, D.,
516 Inoko, H., Yamashiro, K., Ohno-Matsui, K., Matsuo, K., Matsuda, F., Vithana, E.,
517 Seielstad, M., Mizuki, N., Beuerman, R.W., Tai, E.S., Yoshimura, N., Aung, T.,
518 Young, T.L., Wong, T.-Y., Teo, Y.-Y., Saw, S.-M., 2012. Genetic variants on
519 chromosome 1q41 influence ocular axial length and high myopia. PLoS Genet 8,
520 e1002753.
521 Flitcroft, D.I., He, M., Jonas, J.B., Jong, M., Naidoo, K., Ohno-Matsui, K., Rahi, J.,
522 Resnikoff, S., Vitale, S., Yannuzzi, L., 2019. IMI - Defining and Classifying Myopia:
523 A Proposed Set of Standards for Clinical and Epidemiologic Studies. Invest
524 Ophthalmol Vis Sci 60, M20-M30.
525 Haarman, A.E.G., Thiadens, A.A.H.J., van Tienhoven, M., Loudon, S.E., de Klein,
526 J.E.M.M.A., Brosens, E., Polling, J.R., van der Schoot, V., Bouman, A., Kievit,
527 A.J.A., Hoefsloot, L.H., Klaver, C.C.W., Verhoeven, V.J.M., 2022. Whole exome
528 sequencing of known eye genes reveals genetic causes for high myopia. Hum Mol
529 Genet 31, 3290-3298.
530 Harper, A.R., Summers, J.A., 2015. The dynamic sclera: extracellular matrix
531 remodeling in normal ocular growth and myopia development. Exp Eye Res 133, 100-
532 111.
533 Hayden, M.S., Ghosh, S., 2011. NF-κB in immunobiology. Cell Res 21, 223-244.
534 Holden, B.A., Fricke, T.R., Wilson, D.A., Jong, M., Naidoo, K.S., Sankaridurg, P.,
535 Wong, T.Y., Naduvilath, T.J., Resnikoff, S., 2016. Global Prevalence of Myopia and
536 High Myopia and Temporal Trends from 2000 through 2050. Ophthalmology 123,
537 1036-1042.
538 Ikeda, S.-I., Kurihara, T., Jiang, X., Miwa, Y., Lee, D., Serizawa, N., Jeong, H., Mori,

539 K., Katada, Y., Kunimi, H., Ozawa, N., Shoda, C., Ibuki, M., Negishi, K., Torii, H.,
540 Tsubota, K., 2022. Scleral PERK and ATF6 as targets of myopic axial elongation of
541 mouse eyes. Nat Commun 13, 5859.
542 Jimi, E., Fei, H., Nakatomi, C., 2019. NF-κB Signaling Regulates Physiological and
543 Pathological Chondrogenesis. Int J Mol Sci 20.
544 Koga, M., Mizuno, Y., Watanabe, I., Kawakami, H., Goto, T., 2014. Role of VPAC2
545 receptor in monocrotaline-induced pulmonary hypertension in rats. J Appl Physiol
546 (1985) 117, 383-391.
547 Libermann, T.A., Baltimore, D., 1990. Activation of interleukin-6 gene expression
548 through the NF-kappa B transcription factor. Mol Cell Biol 10, 2327-2334.
549 Lin, H.-J., Wei, C.-C., Chang, C.-Y., Chen, T.-H., Hsu, Y.-A., Hsieh, Y.-C., Chen, H.-
550 J., Wan, L., 2016. Role of Chronic Inflammation in Myopia Progression: Clinical
551 Evidence and Experimental Validation. EBioMedicine 10, 269-281.
552 Liu, S., Chen, T., Chen, B., Liu, Y., Lu, X., Li, J., 2022. Lrpap1 deficiency leads to
553 myopia through TGF-β-induced apoptosis in zebrafish. Cell Commun Signal 20, 162.
554 Manavalan, B., Basith, S., Choi, Y.-M., Lee, G., Choi, S., 2010. Structure-function
555 relationship of cytoplasmic and nuclear IκB proteins: an in silico analysis. PLoS One
556 5, e15782.
557 Morgan, M.J., Liu, Z.-g., 2011. Crosstalk of reactive oxygen species and NF-κB
558 signaling. Cell Res 21, 103-115.
559 Qi, J., Pan, W., Peng, T., Zeng, L., Li, X., Chen, Z., Yang, Z., Xu, H., 2022. Higher
560 Circulating Levels of Neutrophils and Basophils Are Linked to Myopic Retinopathy.
561 Int J Mol Sci 24.
562 Saw, S.-M., Gazzard, G., Shih-Yen, E.C., Chua, W.-H., 2005. Myopia and associated
563 pathological complications. Ophthalmic Physiol Opt 25, 381-391.
564 Schippert, R., Burkhardt, E., Feldkaemper, M., Schaeffel, F., 2007. Relative axial
565 myopia in Egr-1 (ZENK) knockout mice. Invest Ophthalmol Vis Sci 48, 11-17.
566 Shi, Y., Li, Y., Zhang, D., Zhang, H., Li, Y., Lu, F., Liu, X., He, F., Gong, B., Cai, L.,
567 Li, R., Liao, S., Ma, S., Lin, H., Cheng, J., Zheng, H., Shan, Y., Chen, B., Hu, J., Jin,
568 X., Zhao, P., Chen, Y., Zhang, Y., Lin, Y., Li, X., Fan, Y., Yang, H., Wang, J., Yang, Z.,

2011. Exome sequencing identifies ZNF644 mutations in high myopia. PLoS Genet 7, e1002084.

Szczerkowska, K.I., Petrezselyova, S., Lindovsky, J., Palkova, M., Dvorak, J., Makovicky, P., Fang, M., Jiang, C., Chen, L., Shi, M., Liu, X., Zhang, J., Kubik-Zahorodna, A., Schuster, B., Beck, I.M., Novosadova, V., Prochazka, J., Sedlacek, R., 2019. Myopia disease mouse models: a missense point mutation (S673G) and a protein-truncating mutation of the Zfp644 mimic human disease phenotype. Cell Biosci 9, 21.

Tang, S.M., Li, F.F., Lu, S.Y., Kam, K.W., Tam, P.O.S., Tham, C.C., Pang, C.P., Yam, J.C.S., Chen, L.J., 2020. Association of the ZC3H11B, ZFHX1B and SNTB1 genes with myopia of different severities. Br J Ophthalmol 104, 1472-1476.

Tedja, M.S., Haarman, A.E.G., Meester-Smoor, M.A., Kaprio, J., Mackey, D.A., Guggenheim, J.A., Hammond, C.J., Verhoeven, V.J.M., Klaver, C.C.W., 2019. IMI - Myopia Genetics Report. Invest Ophthalmol Vis Sci 60.

Tian, Q., Tong, P., Chen, G., Deng, M., Cai, T.e., Tian, R., Zhang, Z., Xia, K., Hu, Z., 2023. GLRA2 gene mutations cause high myopia in humans and mice. J Med Genet 60, 193-203.

Tkatchenko, A.V., Walsh, P.A., Tkatchenko, T.V., Gustincich, S., Raviola, E., 2006. Form deprivation modulates retinal neurogenesis in primate experimental myopia. Proc Natl Acad Sci U S A 103, 4681-4686.

Tkatchenko, T.V., Tkatchenko, A.V., 2019. Pharmacogenomic Approach to Antimyopia Drug Development: Pathways Lead the Way. Trends Pharmacol Sci 40, 833-852.

Tkatchenko, T.V., Troilo, D., Benavente-Perez, A., Tkatchenko, A.V., 2018. Gene expression in response to optical defocus of opposite signs reveals bidirectional mechanism of visually guided eye growth. PLoS Biol 16, e2006021.

Torrealba, N., Vera, R., Fraile, B., Martínez-Onsurbe, P., Paniagua, R., Royuela, M., 2020. TGF-β/PI3K/AKT/mTOR/NF-kB pathway. Clinicopathological features in prostate cancer. Aging Male 23, 801-811.

Wallman, J., Winawer, J., 2004. Homeostasis of eye growth and the question of

599 myopia. Neuron 43, 447-468.
600 Wang, G.-B., Zhang, Q.-J., Xiao, X.-S., Li, J.-Z., Zhang, F.-S., Li, S.-Q., Li, W., Li, T.,
601 Jia, X.-Y., Guo, L., Guo, X.-M., 2004. [Variations of the zinc finger protein 161 gene
602 in Chinese with or without high myopia]. Yi Chuan 26, 155-159.
603 Wu, K.-I.S., Schmid-Schönbein, G.W., 2011. Nuclear factor kappa B and matrix
604 metalloproteinase induced receptor cleavage in the spontaneously hypertensive rat.
605 Hypertension 57, 261-268.
606 Xiao, Q., Xiao, J., Liu, J., Liu, J., Shu, G., Yin, G., 2022. Metformin suppresses the
607 growth of colorectal cancer by targeting INHBA to inhibit TGF-β/PI3K/AKT
608 signaling transduction. Cell Death Dis 13, 202.
609 Yang, E., Yu, J., Liu, X., Chu, H., Li, L., 2023. Familial Whole Exome Sequencing
610 Study of 30 Families With Early-Onset High Myopia. Invest Ophthalmol Vis Sci 64,
611 10.
612 Ye, M., Ma, Y., Qin, Y.-X., Cai, B., Ma, L.-M., Ma, Z., Liu, Y., Jin, Z.-B., Zhuang, W.-
613 J., 2023. Mutational investigation of 17 causative genes in a cohort of 113 families
614 with nonsyndromic early-onset high myopia in northwestern China. Mol Genet
615 Genomics 298, 669-682.
616 Yoshida, M., Whitsett, J.A., 2006. Alveolar macrophages and emphysema in
617 surfactant protein-D-deficient mice. Respirology 11 Suppl, S37-S40.
618 Younis, S., Jouneau, A., Larsson, M., Oudin, J.F., Adenot, P., Omar, J., Brochard, V.,
619 Andersson, L., 2023. Ablation of ZC3H11A causes early embryonic lethality and
620 dysregulation of metabolic processes. Proc Natl Acad Sci U S A 120, e2216799120.
621 Younis, S., Kamel, W., Falkeborn, T., Wang, H., Yu, D., Daniels, R., Essand, M.,
622 Hinkula, J., Akusjärvi, G., Andersson, L., 2018. Multiple nuclear-replicating viruses
623 require the stress-induced protein ZC3H11A for efficient growth. Proc Natl Acad Sci
624 U S A 115, E3808-E3816.
625 Zhao, F., Zhou, Q., Reinach, P.S., Yang, J., Ma, L., Wang, X., Wen, Y., Srinivasalu, N.,
626 Qu, J., Zhou, X., 2018. Cause and Effect Relationship between Changes in Scleral
627 Matrix Metallopeptidase-2 Expression and Myopia Development in Mice. Am J
628 Pathol 188, 1754-1767.

Table 1 The clinical features and mutations of affected patients

ID.	Sex	Age	Refraction (D)		Axial length (mm)		Genotype
			OD	OS	OD	OS	
1	M	18	-6.50	-5.125	25.68	25.34	c.412G>A:p.Val138Ile, Het
2	F	15	-4.25	-6.125	24.61	25.11	c.128G>A:p.Gly43Glu, Het
3	M	17	-8.00	-8.75	26.16	27.02	c.461C>T :p.Pro154Leu, Het
4	F	15	-6.25	-3.7	25.53	24.86	c.2239T>A:p.Ser747Thr, Het

M, male; F, female; Het, heterozygote; OD, ocular dexter; OS, oculus sinister.

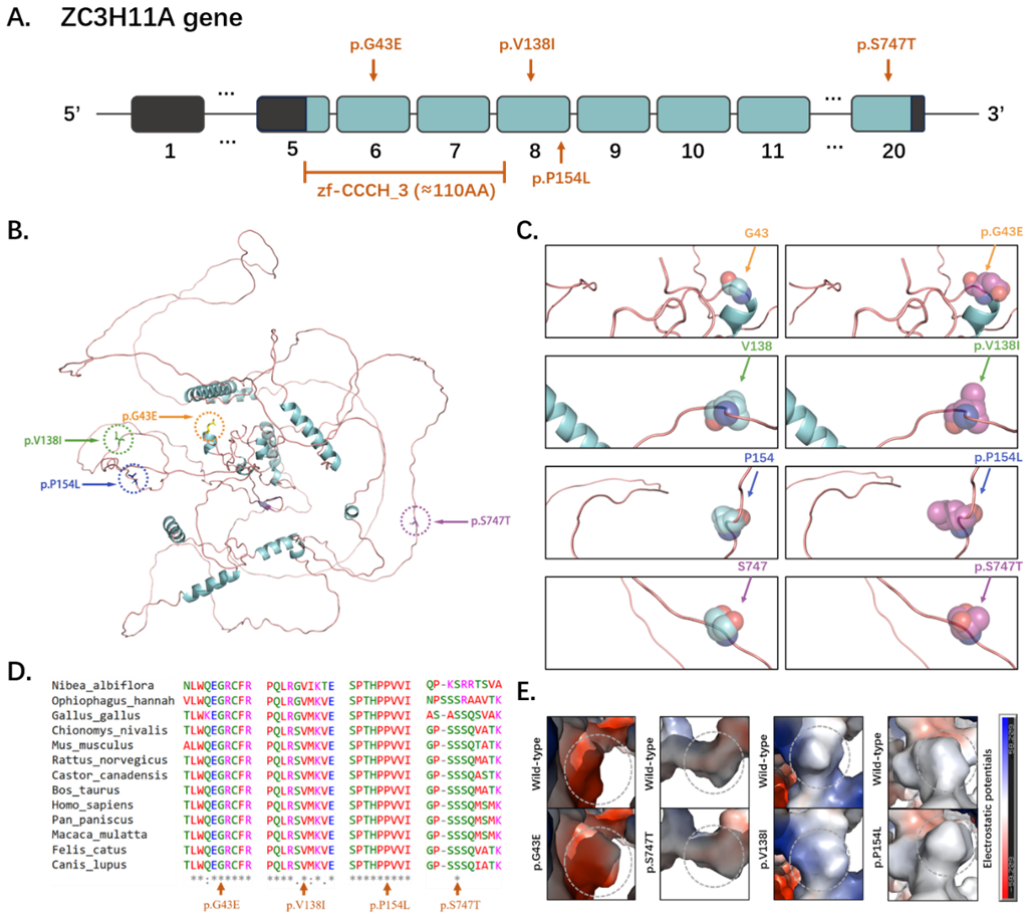

Figure 1. Structural modelling of ZC3H11A gene mutations. (A) Illustration of exons and mutation sites of ZC3H11A; exons 5-8 of ZC3H11A encode the zf-CCCH_3 protein domain. (B) A structural model of the full-length human ZC3H11A protein was generated using PyMOL; the locations of the four mutation sites are marked. (C) The p.G43E mutation is located in exon 6, while the p.V138I and p.P154L mutations are in exon 8, and the p.S747T mutation is in exon 20. (D)

639 Multiple sequence alignment of the proteins where ZC3H11A mutations are found in
640 multiple species. (E) These mutations can result in a higher degree of conformational
641 flexibility at the corresponding sites, potentially destabilizing the structural domain.
642

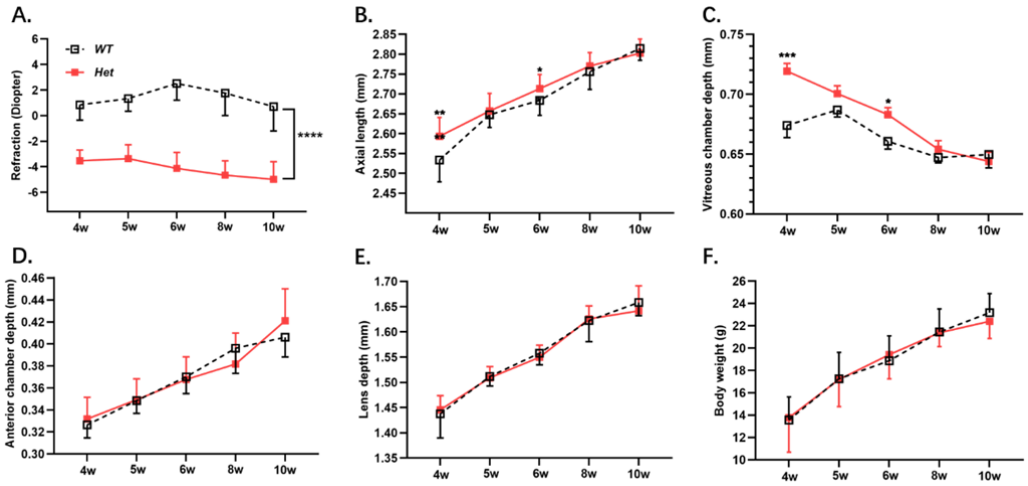

643
644 **Figure 2. Comparison of ocular biometrics and body weights of Zc3h11a Het-KO**
645 **(n=14) and WT (n=10) littermates during weeks 4-10 of development.** (A, B)
646 Refraction and axial length in Zc3h11a Het-KO mice. (C) Vitreous chamber depth.
647 (D-F) Anterior chamber depth, lens depth and body weight. The effect of genotype on
648 time-dependent refractive development was assessed through independent samples t-
649 tests. P-values are indicated as follows: *P<0.05, **P<0.01, ***P<0.001 and
650 ****<0.0001.
651

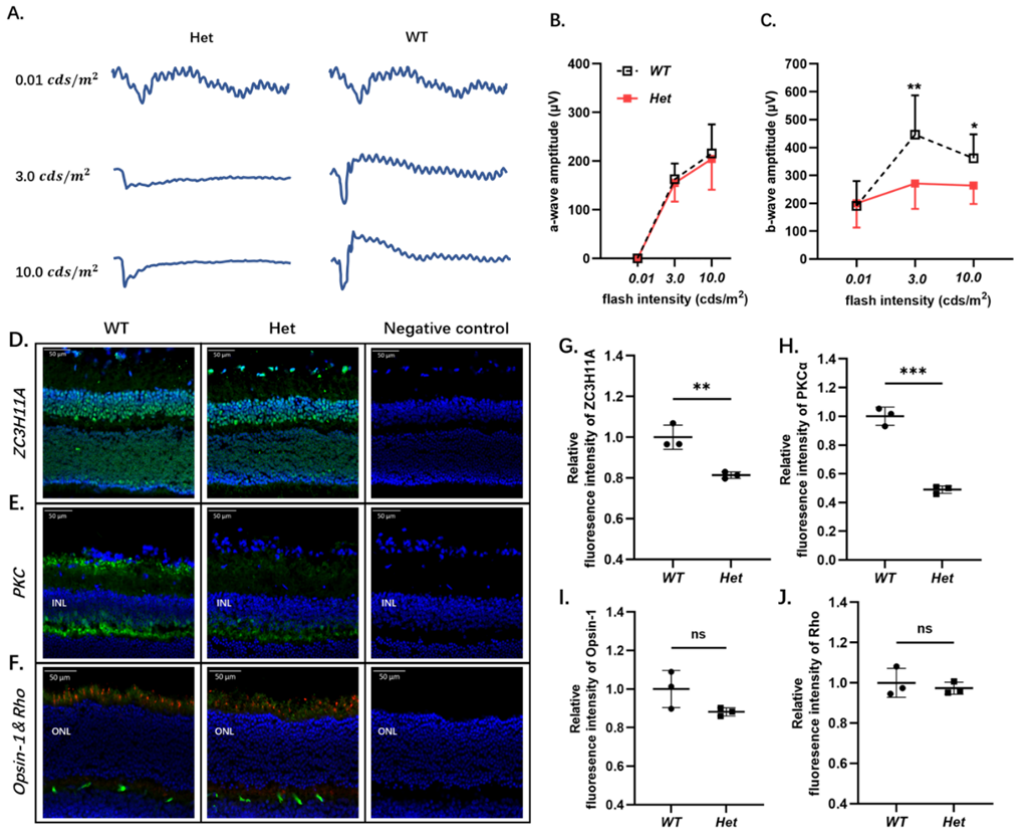

Figure 3. Electroretinography and immunohistochemical localization of Zc3h11a, PKCα, Opsin-1 and Rhodopsin in WT and Het-KO mice eyes. (A) Representative scotopic ERG responses from Het-KO and WT eyes at dark 0.01, 3.0 and 10.0 cds/m^2. (B, C) Statistical analysis of a-wave and b-wave amplitudes. Mean ± standard deviation, n=12/group. (D-F) Immunofluorescence-stained samples to detect Zc3h11a, bipolar cells, cone and rod cells. (G, H) Lower levels of Zc3h11a and PKCα (E. H) expression were observed in Het-KO mice (I, J) The expression levels of Opsin-1 and Rhodopsin between Het-KO and WT mice. Statistical significance was defined as *P < 0.05, **P<0.01 and ***P<0.001, as determined by independent samples t-tests.

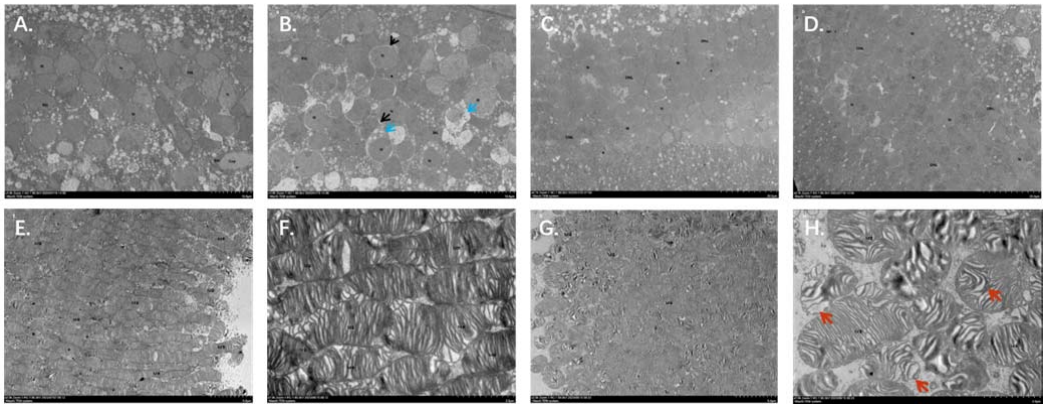

Figure 4. TEM showing the retinal ultrastructure of WT and Het-KO mice. (A, B) Cellular morphology of the INL in which bipolar cells are located in WT (A) and Het-KO mice (B). (C, D) Cellular morphology of the ONL in which the optic cells are located in WT (C) and Het-KO mice (D). (E, F) MB structure in WT mice. (G, H) MB structure of Het-KO mice.

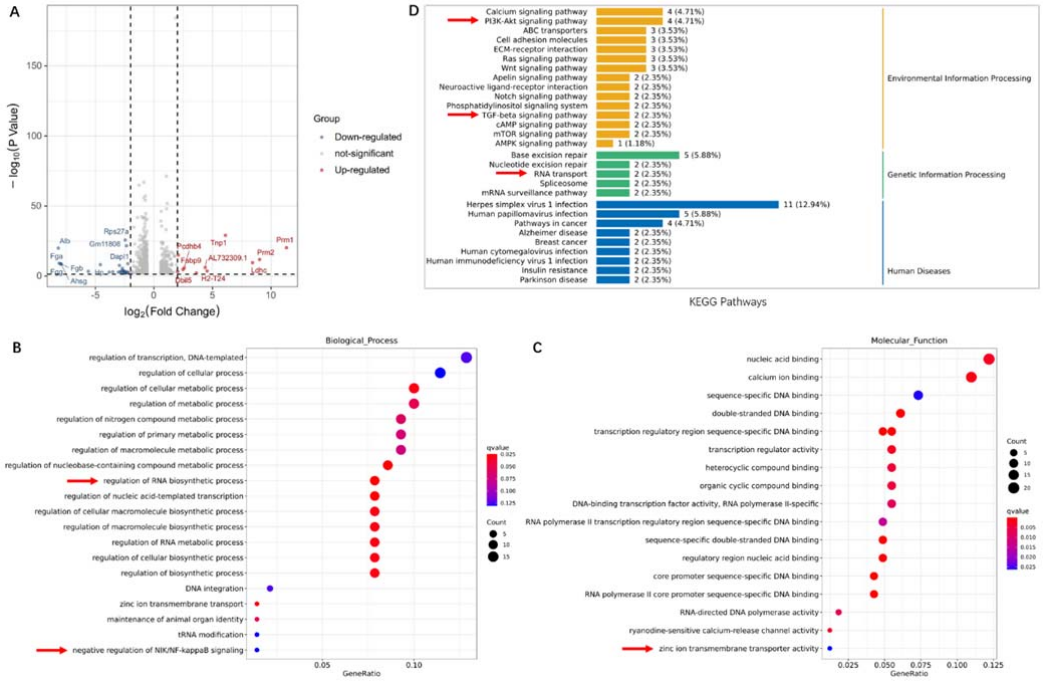

Figure 5. RNA-Seq analysis of molecular and pathway differences between WT control and Het-KO retinas. (A, B) Volcano maps were utilized to visualize the differentially expressed genes (DEGs) between WT control and Het-KO mouse retinas. (C, D) GO enrichment analysis of DEGs in the Het-KO group (E) KEGG pathway enrichment analysis of DEGs in the Het-KO group.

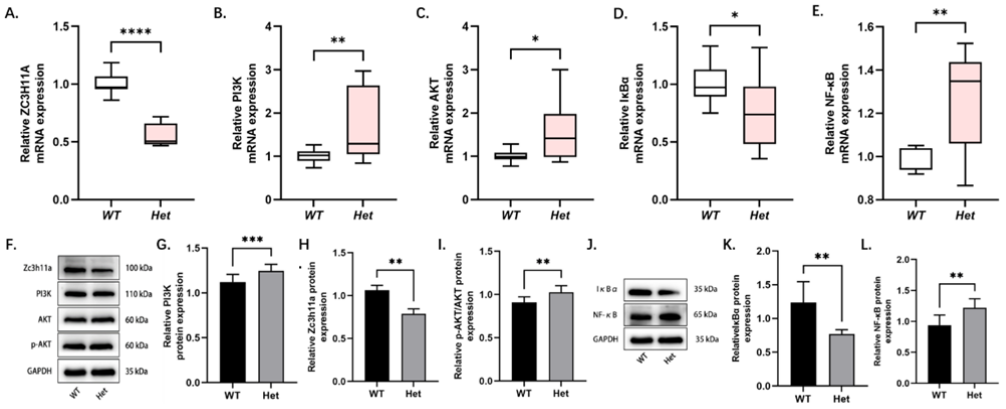

Figure 6. Effect of Zc3h11a on the expression of genes and proteins related to the PI3K-AKT and NF-κB signalling pathways in the retina. (A-C) The ZC3H11A, PI3K and AKT gene levels (n=3) were evaluated. (D, E) The IκBα and NF-κB gene levels (n=3). (F) Protein expression levels of ZC3H11A, PI3K, AKT, p-AKT and GAPDH were detected by western blot. (G-I) Quantitative analysis of the ZC3H11A and PI3K levels were normalized to GAPDH, while p-AKT levels were normalized to AKT (n=3). (J) The protein expression levels of IκBα, NF-κB and GAPDH were determined by western blot analysis. (K, L) Quantitative analyses of IκBα and NF-κB were normalized to GAPDH (n=3).

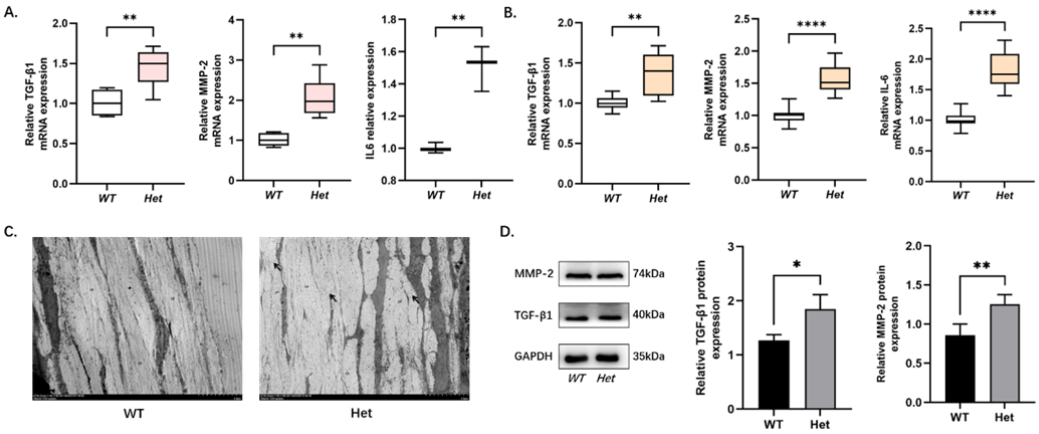

Figure 7. **Effect of Zc3h11a on the expression of TGF-β1, MMP-2 and IL-6 in the retina and sclera.** (A, B) Examination of TGF-β1, MMP-2 and IL-6 gene expression in the sclera (A) and retina (B) (n=3). (C) TEM structure of sclera. (D) Determination of TGF-β1 and MMP-2 protein expression levels, normalized to GAPDH, through western blot analysis (n=3).

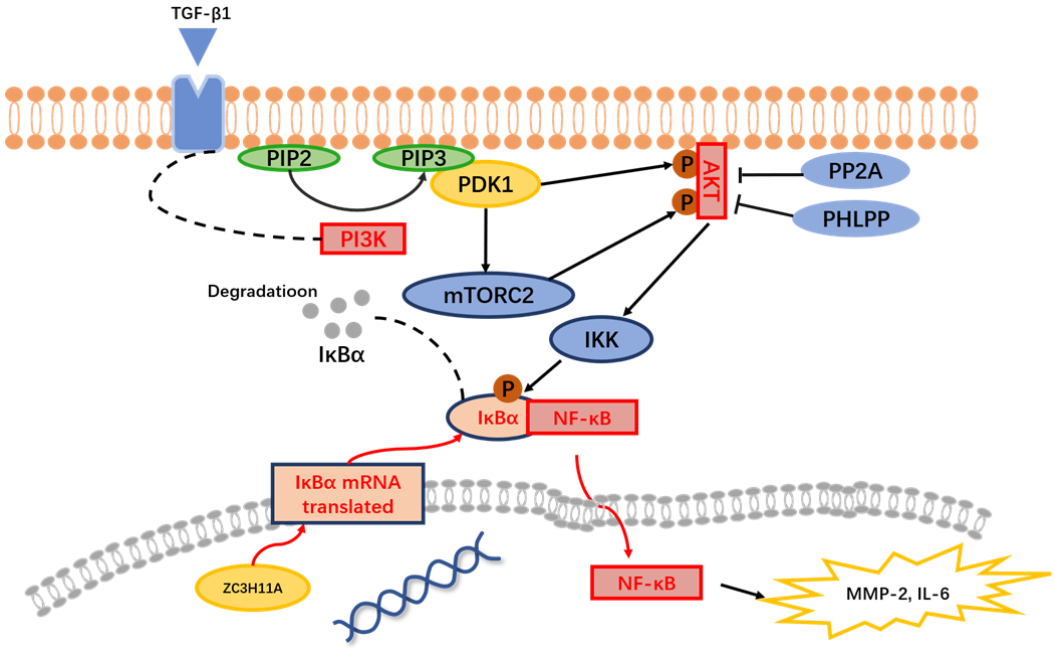

690

691 **Figure 8. Schematic representation of the PI3K-AKT-NF-κB signalling pathway**

692 **in retina.**

693

694

695

696

697

698

699

700

701

702

703

704

705

706

707

708

709 **Supplementary files**

710

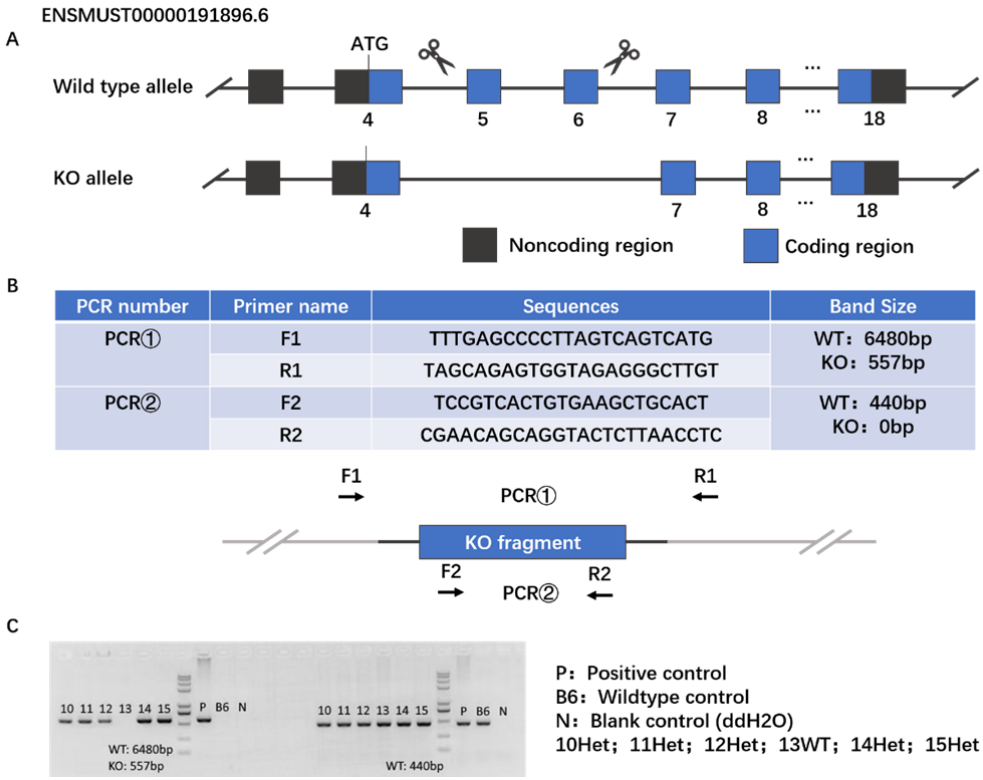

PCR number	Primer name	Sequences	Band Size
PCR①	F1	TTTGAGCCCCTTAGTCAGTCATG	WT：6480bp KO：557bp
	R1	TAGCAGAGTGGTAGAGGGCTTGT	
PCR②	F2	TCCGTCACTGTGAAGCTGCACT	WT：440bp KO：0bp
	R2	CGAACAGCAGGTACTCTTAACCTC	

711 **Figure supplement 1. Generation of Zc3h11a KO mice.** (A) Generation of Zc3h11a

712 KO mice in C57BL/6J background using CRISPR/Cas9 technology. (B-C) Primers

713 for genotyping and examples of genotyping results of Zc3h11a Het-KO mice and

714 wild-type mice

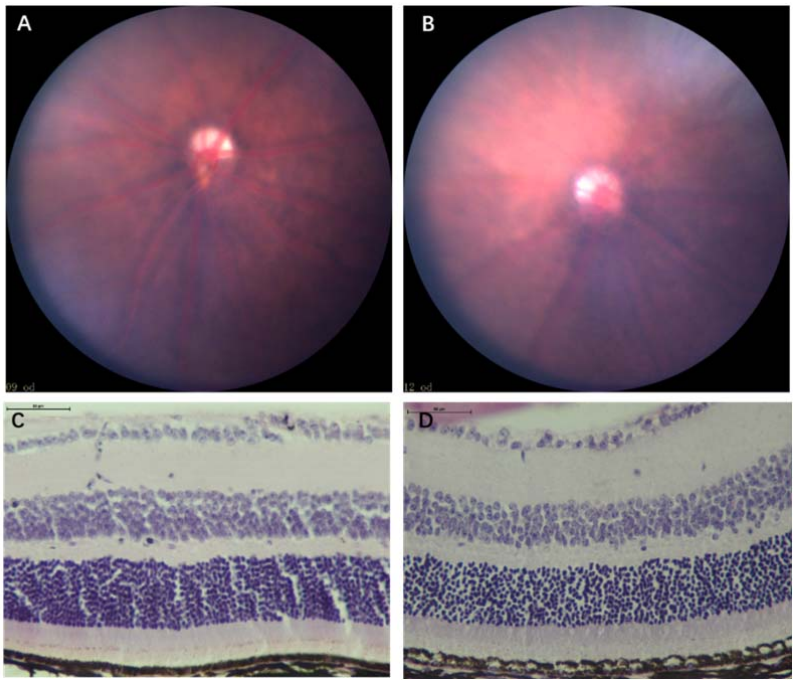

Figure supplement 2. Fundus photographs and HE staining of Het and WT mice at 8th week. (A. B) Fundus photographs of WT (A) and Het-KO mice (B) (n=3). (C. D) HE staining of retina in WT (C) and Het-KO mice (D) (n=3).

Table supplement 1. Sequence of oligonucleotides

Gene	Sequence
ZC3H11A	Forward: CTAAACTGCGCTTTCCATCACA Reserve: CGTTGATTACAACAGGCGGAT
PI3K	Forward: TGGGACCTTTTTGGTACGAGA Reserve: AGCTAAAGACTCATTCCGGTAGT
AKT	Forward: CCTTTATTGGCTACAAGGAACGG Reserve: GAAGGTGCGCTCAATGACTG
IκBα	Forward: TGAAGGACGAGGAGTACGAGC Reserve: TGCAGGAACGAGTCTCCGT
NF-κB	Forward: GGGGCCTGCAAAGGTTATC Reserve: TGCTGTTACGGTGCATACCC
TGF-β1	Forward: GTAACGCCAGCCAGGAATTGTTGCTA Reserve: CTTCAATACGTCAGACATTCGGG
IL-6	Forward: CTGCAAGAGACTTCCATCCAG Reserve: AGTGGTATAGACAGGTCTGTTGG
MMP-2	Forward: CAAGTTCCCCGGCGATGTC Reserve: TTCTGGTCAAGGTCACCTGTC
GAPDH	Forward: AGGTCGGTGTGAACGGCTTTG Reserve: TGTAGACCATCTAGTTGAGGTCA

The mRNA expression levels were analysed by the comparative $2^{-\Delta\Delta}$ Ct method and normalised using GAPDH.